Analysis of Al$_2$O$_3$-ZrO$_2$ ceramic insert in turning process of Ti-6Al-4V alloy using grey Taguchi-based response surface methodology (GT-RSM)

H. Patel[1]**, H. Patil*[1]

[1]*GIDC Degree Engineering College, Mechanical Engineering Department, Navsari, Gujarat, India*

Abstract

The present investigation aimed at a sustainable green turning operation of Ti-6Al-4V alloy using multi-objective optimization of surface roughness, tool flank wear, material removal rate, and tool wear loss with cutting speed, feed rate, and depth of cut as input parameters. The experiments were performed on a CNC lathe machine using an alumina-zirconia (Al$_2$O$_3$-ZrO$_2$) ceramic insert under a dry machining environment. The experiments were performed to examine the influence of input parameters with three levels and their interactions on the output responses. The experiment trials were designed according to Taguchi's L$_{25}$ orthogonal array. A hybrid approach of grey Taguchi-based response surface methodology (GT-RSM) was exposed for estimating the optimal integration of turning parameters. The weights to the output characteristics were assigned by the analytical hierarchy process (AHP). According to the ANOVA, cutting speed was the most influencing factor in the grey relation grade (GRG) succeeded by the depth of cut and feed rate. The optimized turning settings improved the surface roughness, tool flank wear, and tool wear loss by 10.31%, 6.51%, and 7.69% respectively with a 2.21% decrease in material removal rate. The result indicated that the GT-RSM methodology provided an excellent database that was effective to enhance the output quality responses.

Keywords: dry machining, alumina-zirconia (Al$_2$O$_3$-ZrO$_2$) ceramic insert, hybrid methodology, analytical hierarchy process (AHP), ANOVA.

INTRODUCTION

In modern manufacturing processes, the cost burden on the machining process has led to an exhaustive investigation of traditional coolants used in the majority of machining processes. The costs associated with the use of coolant range from 7% to 17% of the total machining process costs [1]. Furthermore, the workplace in the manufacturing industries is not clean, safe, and healthy. Current technological trends suggest that this condition will not be sustainable in the future and that a systematic approach would be expected to address the strict environmental rules [2]. The cost of manufacturing and the environmental impact of coolants can be considerably reduced by discontinuing the coolants and by adopting dry machining or minimum quantity lubrication (MQL) technologies [3]. The decrease in significant coolant hazards at work can improve manufacturing process performance, worker safety, cost, quality, and job satisfaction [4]. The machining process of material can lead to heat generation in the cutting zone because of friction. During machining, cutting fluids can govern the adverse effects of friction, temperature rise, tool-workpiece adherence, and chip flushing [5]. As a result, the use of cutting fluids has been considered an important element of the metal cutting processes to achieve a robust machining process, increased tool life, and an excellent surface finish. Coolants release harmful fumes and bad odors can cause skin irritations and have an adverse effect on operators and the environment

[6]. Manufacturing industries were somewhat effective to decrease coolant effects by adopting minimum quantity lubrication (MQL) or mist lubrication [7]. The mist can have a negative impact on the operator's respiratory system. The difficulty of acquiring, supplying, collecting, injecting, controlling, and dismantling cutting fluids results in higher overhead expenses [8].

Dry machining is a feasible alternative for a cost-effective and safe machining process. The use of effective dry machining requires studying and assessing the cutting process mechanisms, cutting tool material, cutting tool design, and their associated equipment [9]. Dry machining cannot be executed just by cutting off the coolant feed. Dry machining requires an extensive understanding of both the cutting tool and the workpiece materials [10]. Dry cutting is convenient when using a larger positive rake angle on a submicron WC-Co tool, which considerably decreases the overall cutting energy [11], a tool having high hot hardness and hence able to withstand high cutting temperatures, application of coatings on the cutting tool to serve as a friction-reducing surface layer to resist the temperature, and decreasing cutting speed to achieve longer tool life and cost efficiency [12]. The use of a large positive rake angle and a slower cutting speed cannot outweigh the advantages because it reduces tool strength, tool life, and productivity. On the other hand, cutting tool coatings can be drawn out, which do not provide the sufficient productivity demanded in the modern machining process. The ceramic refractory cutting tools are capable to sustain very high temperatures (around 1200 °C) and yield long tool life at high cutting speeds. For effective turning of hard-to-cut materials, many researchers have carried out comprehensive experimental

*hari.mech.patel@gmail.com

https://orcid.org/0000-0001-5999-7990

work employing alumina-based ceramics [13], silicon nitride-based ceramics [14], cermet-based ceramics [15], and SiAlON-based ceramics [16]. Ceramic coatings and texturing of ceramic tools are the focus of most experimental efforts and testing of machining behavior [17, 18]. Alumina-zirconia (Al_2O_3-ZrO_2) ceramic insert tool is used in this experimental study.

Titanium alloys have excellent properties like low density, resistance to corrosion, high specific strength, and superior fracture toughness making them more popular in aerospace, marine, automobile, and defense sectors. Titanium alloys have a low elastic modulus and low heat conductivity, making them hard to cut [19]. Ceramic cutting tools have high wear resistance, good compressive strength, and high chemical stability, making them successively adopted for machining hard-to-cut materials with excellent surface integration and high machining performance [20]. However, due to catastrophic failure, low toughness, and brittle fracture, ceramic cutting tools have not been adopted widely in the manufacturing industry. As a result, for improved toughness and strength in ceramics, the microstructural arrangement has been a significant factor in manufacturing structural ceramics. One approach of ceramic toughening mechanism is governing a processing region around the crack tip, the other approach is involving reinforcements (particulates, fibers, whiskers, etc.) for crack bridging, and another is the transformation toughening regulated by grain size, grain size distribution, and stabilizing concentrations [21, 22]. A stabilized tetragonal zirconia (t-ZrO_2) based structural ceramics are extensively utilized in the cutting tool, bearing components, biomedical field, and other various application domains because of their high fracture toughness and strength predicted on martensitic tetragonal to monoclinic (t→m) transformation [23]. However, at room temperature t-ZrO_2 is not stable [24]. The three primary zirconia polymorphic phases are m-ZrO_2, t-ZrO_2, and c-ZrO_2. Kuwabara et al. [25] effectively estimated the Helmholtz free energies of t-ZrO_2 and m-ZrO_2 and revealed that t-ZrO_2 becomes more stable than m-ZrO_2 at a temperature over 1350 K and it requires more research to bridge link between phase structures and charge properties. The instability of t-ZrO_2 ceramics under certain conditions can cause immediate transformation of t-ZrO_2→m-ZrO_2 [26]. The stability of zirconia-based ceramics can be improved by the production of ceramics that are less susceptive to the negative t→m transformation effects. In zirconia toughened alumina (ZTA), it is possible to slow down this phase transformation due to the stiff alumina matrix [27]. Yttria is the most effective stabilizer to obtain the tetragonal phase in zirconia ceramics and results in superior mechanical properties and wear characteristics, and has an effect on tetragonal phase transformability [28]. Shin et al. [29] investigated t→m transformation in three types of Al_2O_3-ZrO_2, synthesized without additives or with yttria as a tetragonal phase stabilizer. They found that the toughness improvement was because of t→m transformation, attributed to the volume fraction of m-ZrO_2 transformation in fracture. Szutkowska [30] evaluated the influence of unstabilized or 10 vol% yttria-stabilized ZrO_2 in an Al_2O_3. By comparing both results, the yttria-stabilized ZrO_2 has stabilized the tetragonal phase, as a result, a lower amount of ZrO_2 contributes to the toughening improvement from t to m transformations. The reviews imply that the toughening mechanism and the toughness-strength correlations are governed by the microstructure, type, and content of ZrO_2, the grain size of both Al_2O_3 and ZrO_2, and the ZrO_2 particle positions. The yttria-stabilized ZrO_2-toughened-Al_2O_3 has induced significant observations as a way to improve machining performances. In this experimental work, 3Y-ZTA was chosen as a ceramic cutting insert.

There has been little research reported on solid ceramic insert tools during turning operation. The ceramic cutting tool can attain a temperature of around 1200 °C when machining titanium alloys, affecting the tool material properties and increasing tool wear [31]. Grguraš and Kern [32] performed machining operations on hard-to-cut material using ceramic and carbide tools. They revealed that in comparison to carbide tools, ceramic tools can enhance the performance and production rate. Chen et al. [33] performed high-speed machining of Ti-6Al-4V with TiB_2-B_4C ceramic tool to study wear mechanism and cutting performance. Ceramic cutting tools with higher TiB_2 content may have better-cutting performance and longer tool life in the cutting of Ti-6Al-4V alloys as compared to WC cutting tools. Tian et al. [34] prepared a graded Si_3N_4 [Si_3N_4/(W,Ti) C/Co] ceramic tool for turning a GH2132 iron-based alloy, which demonstrated enhanced thermal and mechanical shock resistance compared to the homogeneous reference tool. This is because of the evolution of residual compressive stress, which reduces the stresses resulting from external loading and reduces the driving force for crack propagation. Altin et al. [35] studied the influence of the input parameters while machining nickel-based hard-to-cut alloy using ceramic tools on tool tribology and service life. The square type Al_2O_3+SiC_w ceramic tool was found to be effective for low-cutting speeds, while the round type insert was found to be good for high-cutting rates. Zeilmann et al. [36] investigated the tribological behavior of ceramic tools in dry and wet Inconel 718 turning and deduced that the notch wear for SiAlON tools was observed less using coolants, while in dry turning using Al_2O_3+SiC_w insert performance improved. It can be noted that previous research largely focused on cutting superalloys using nitrides, SiAlON, and cermets-based ceramic tools, while only a little amount of work has been noted on alumina-based ceramic tools, especially alumina-zirconia based ceramic tools.

Numerous decision-making methodologies, such as the analytic hierarchy process (AHP), a technique for order of preference by similarity to ideal solution (TOPSIS) [37], entropy weight method (EWM) [38], data envelopment analysis based ranking (DEAR), grey relational analysis (GRA) [39], and multi-objective optimization method by ratio analysis (MOORA) [40], have been suggested in the literature to investigate the multiple criteria involved with turning operation. GRA methodology converts multi-objective

optimization problems into a single objective function. To evaluate several responses in GRA, a grey relational grade is created to determine the measure of similarity among sequences. Tzeng et al. [41] and Singh et al. [42] used the GRA methodology to optimize the turning operation. GRA was used in the drilling process of composites by Haq et al. [43] and Rajmohan and Palanikumar [44] to optimize multi-response output. The traditional method involves a large series of experiments and it also does not consider the interacting effects between input variables. Response surface methodology (RSM) is a convenient method for developing mathematical models since it requires fewer tests and so saves money and time [45]. Hybrid methodology, for optimizing responses in various contexts, incorporates two techniques; a combination strategy was established to take the benefits of the methodologies included in the research work [46].

This work aimed to optimize the turning process parameters of Ti-6Al-4V alloy in a dry machining environment. The experiments were performed as per Taguchi's L_{25} orthogonal array on CNC (computerized numerical control) machine using alumina-zirconia (Al_2O_3-ZrO_2) ceramic insert with cutting speed, feed rate, and depth of cut as input parameters while surface roughness, tool flank wear, materials removal rate, and tool wear loss as multi-output responses. Subsequently, GRA methodology with the AHP weight assign method was employed to optimize

the multi-responses. ANOVA was used to determine the significance of each parameter in the turning operation. The output attribute turning operations were examined and a hybrid methodology of grey Taguchi-based response surface methodology (GT-RSM) was presented for predicting the optimum machining condition. The quadratic mathematical model using RSM was developed. The validity and fitness of the developed model were tested. Finally, a confirmation experiment was performed using the optimum levels of input turning parameters to demonstrate the enhancement of the performance measure, namely the grey relational grade.

MATERIALS AND METHODOLOGY

Turning process: Ti-6Al-4V grade 5 (Plus Metals, India) alloy bar with a length of 220 mm and a diameter of 40 mm was used as the workpiece in the experiments. The chemical composition and mechanical properties of Ti-6Al-4V (grade 5) alloy is presented in Tables I and II, respectively. The scanning electron microscopy (SEM, Evo 500, Zeiss) micrograph and energy dispersive spectroscopy (EDS) spectrum of the Ti-6Al-4V alloy are shown in Fig. 1. The turning experiments were performed on a three-axis CNC machine (Uniturn 500, Gedee Weiler) with different input cutting parameters. The turning experiments under a dry cutting environment were performed by alumina-zirconia (Al_2O_3-ZrO_2) ceramic insert (grade SZ 200, Union

Table I - Chemical composition of the Ti-6Al-4 V (grade 5) alloy.

Ti	Al	V	Fe	O
90%	6%	4%	0.25%	0.2%

Table II - Physical and mechanical properties of Ti-6Al-4V (grade 5) alloy.

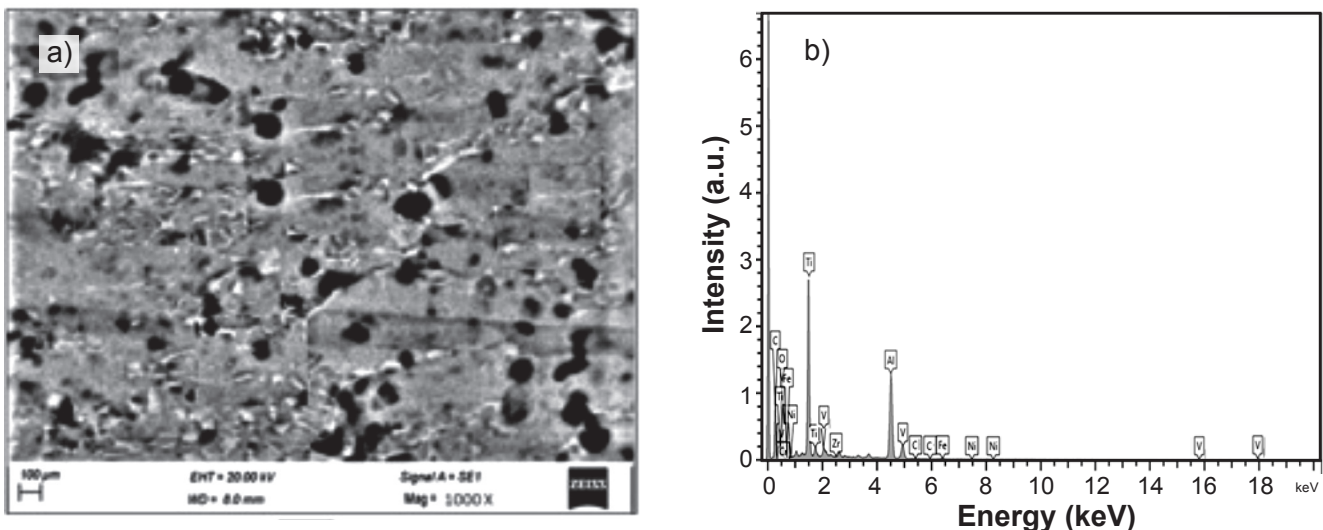| Density (g/cm³)	Vickers hardness	Ultimate tensile strength (MPa)	Modulus of elasticity (GPa)	Fracture toughness (MPa.m$^{1/2}$)
4.43	349	900	114	43

Figure 1: SEM micrograph (a) and EDS spectrum (b) of Ti-6Al-4V alloy.

Table III - Physical and mechanical properties of the alumina-zirconia (Al_2O_3-ZrO_2) ceramic insert.

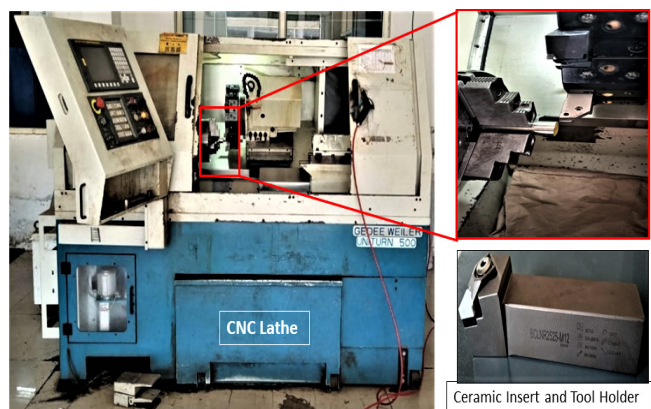| Color	Density (g/cm³)	Vickers hardness	Fracture toughness ($MPa.m^{1/2}$)	Thermal conductivity ($cal.m^{-1}.s^{-1}.°C^{-1}$)
White	4	1800	4.50	0.07

Figure 2: Images of experimental set-up for turning Ti-6Al-4V alloy in a CNC machine.

Mater., South Korea) having 20% 3Y-ZrO_2 and 80% Al_2O_3. The ceramic insert used had ISO designation CNGN 120408 E40 with rhombic shape, 0° rake angle, and with no chip breaker. Its properties are presented in Table III. The experimental setup used to perform turning operations on the CNC machine is shown in Fig. 2. SEM micrograph and EDS spectrum of the alumina-zirconia ceramic insert are shown in Fig. 3. The chemical composition of the alumina-zirconia ceramic insert is shown in Table IV.

The CNC machine had a spindle rotation speed range from 50 to 4000 rpm (revolutions per minute) with a 7.5 kW motor drive. The input parameters adopted for the trails were the cutting speed (v) in rpm, feed rate (f) in mm/rev., and depth of cut (d) in mm. The numbers of input parameters with their chosen levels for the work are presented in Table V. The experiment runs were performed using Taguchi's L_{25} factorial design. Each experiment trail was carried out at random by a new insert, and the trails were replicated twice to ensure data consistency and to average out the influence of uncontrollable variables. The output responses measured for the different experimental runs included surface roughness (SR), tool flank wear (TFW), material removal rate (MRR), and tool wear loss (TWL). The surface roughness tester (TR-200, Time) was used to measure the roughness of the
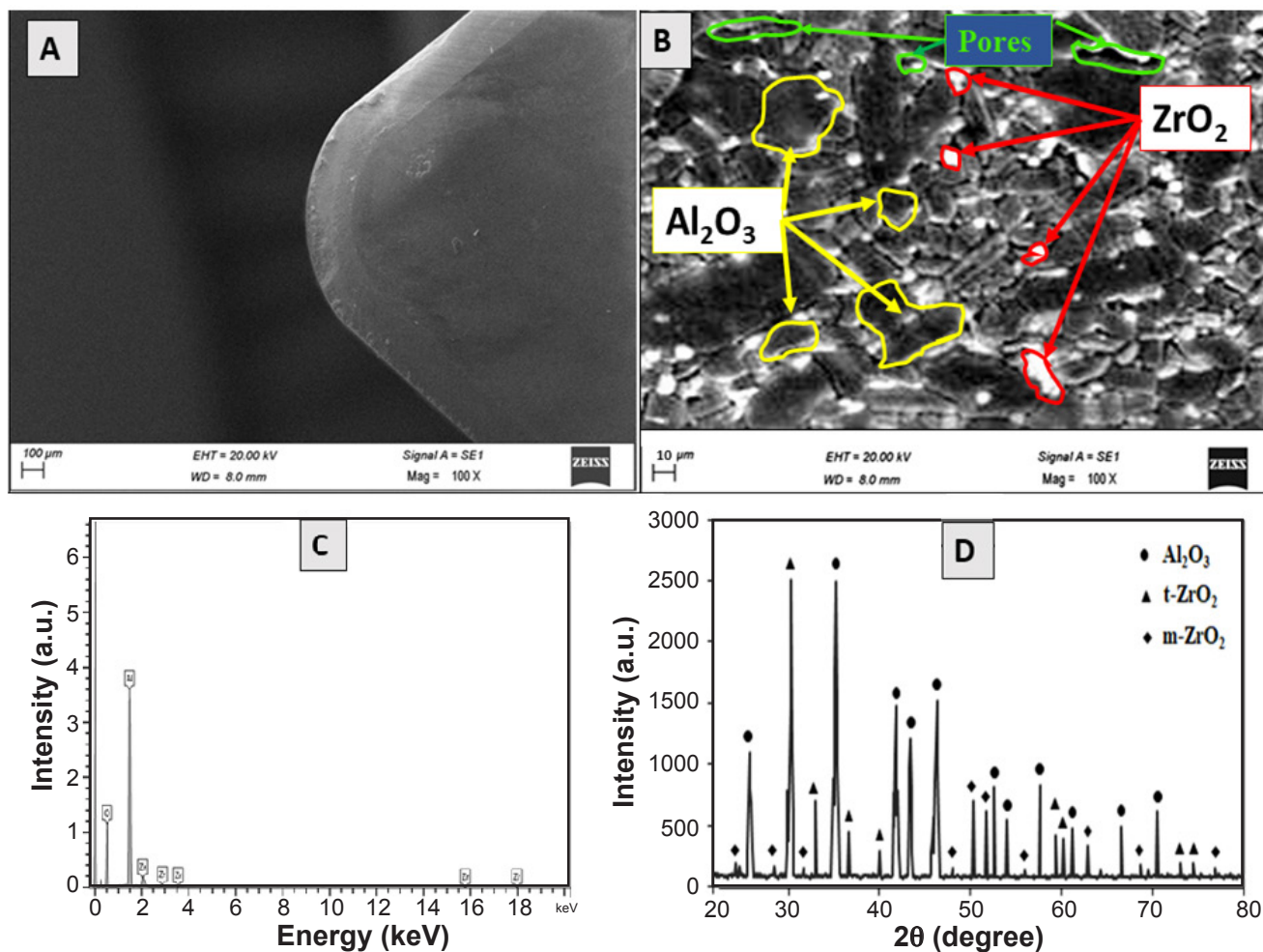

Figure 3: SEM micrographs (a,b), EDS spectrum (c), and X-ray diffraction pattern (d) of alumina-zirconia (Al_2O_3-ZrO_2) ceramic insert tool.

turned surface. The tool flank wear of the ceramic insert used in every cutting experiment was measured using a tool maker's microscope (RT 500, Radical). The tool wear loss (TWL) was calculated by using a laboratory weight measuring machine (CWS Series, Scale-Tec, precision ±0.001 g) to measure the weight of the ceramic tool before

and after the experiment. A conventional equation was used to calculate the material removal rate. Table VI represents the layout of experiment runs as per Taguchi's L_{25} orthogonal array design with their measured responses. The responses were measured twice and their average value accounted to minimize the inaccuracy in the observed measurements.

Cutting tool characterization: SEM micrograph (Fig. 3b) showed that the $3Y-ZrO_2$ was uniformly distributed in Al_2O_3. The grain sizes of Al_2O_3 and $3Y-ZrO_2$ ranged from 1-7 μm and 0.2-1 μm, respectively. Fig. 3d shows the X-ray diffraction (XRD) pattern of the $Al_2O_3-ZrO_2$ ceramic insert, which presented Al_2O_3, $t-ZrO_2$, and $m-ZrO_2$. The main phase

Table IV **-** Chemical composition of the alumina-zirconia ($Al_2O_3-ZrO_2$) ceramic insert.

Al	Zr	O
45.58%	9.57%	44.85%

Table V - Machining parameters with their levels.

Machining parameter	Symbol	Unit	Level 1	Level 2	Level 3	Level 4	Level 5
Cutting speed	v	rpm	3500	3625	3750	3875	4000
Feed rate	f	mm/rev.	0.05	0.10	0.15	0.20	0.25
Depth of cut	d	mm	0.1	0.2	0.3	0.4	0.5

Table VI - Experiment runs as per L_{25} orthogonal array and the measured responses.

| Exp. No.	Cutting speed (rpm)	Feed rate (mm/rev.)	Depth of cut (mm)	Surface roughness (μm)	Tool flank wear (mm)	Material removal rate (mm³/s)	Tool wear loss (g)
1	3500	0.05	0.1	0.600	1.118	1.512	0.021
2	3500	0.10	0.2	0.633	1.182	6.006	0.043
3	3500	0.15	0.3	0.744	1.232	13.315	0.063
4	3500	0.20	0.4	0.814	1.311	24.640	0.071
5	3500	0.25	0.5	0.959	1.374	37.400	0.071
6	3625	0.05	0.4	0.459	1.419	5.970	0.065
7	3625	0.10	0.5	0.596	1.463	14.469	0.093
8	3625	0.15	0.1	0.456	1.264	4.170	0.033
9	3625	0.20	0.2	0.525	1.318	11.028	0.042
10	3625	0.25	0.3	0.618	1.381	20.336	0.050
11	3750	0.05	0.2	0.392	1.363	2.734	0.061
12	3750	0.10	0.3	0.497	1.434	8.061	0.079
13	3750	0.15	0.4	0.547	1.492	15.699	0.087
14	3750	0.20	0.5	0.617	1.517	25.221	0.099
15	3750	0.25	0.1	0.459	1.325	6.011	0.039
16	3875	0.05	0.5	0.390	1.598	6.150	0.107
17	3875	0.10	0.1	0.358	1.391	2.338	0.045
18	3875	0.15	0.2	0.403	1.439	10.413	0.068
19	3875	0.20	0.3	0.480	1.502	13.445	0.082
20	3875	0.25	0.4	0.551	1.569	21.678	0.098
21	4000	0.05	0.3	0.285	1.529	3.206	0.082
22	4000	0.10	0.4	0.339	1.594	8.247	0.103
23	4000	0.15	0.5	0.400	1.619	14.709	0.112
24	4000	0.20	0.1	0.291	1.412	3.671	0.052
25	4000	0.25	0.2	0.347	1.484	9.051	0.064
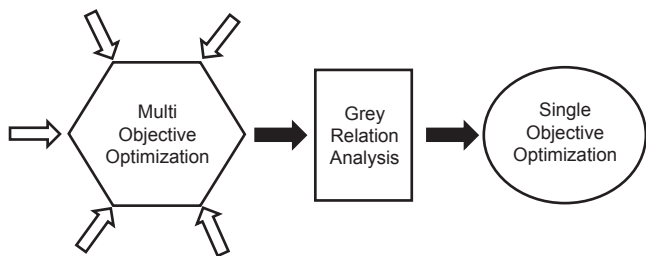
Figure 4: Schematic of the plan of grey relational analysis.

of the sample, α-Al$_2$O$_3$, had peaks at 2θ= 25.7°, 35.2°, 41.8°, 43.4°, 46.3°, 52.6°, 57.6°, 61.3°, 66.6°, 70.5°, 74.5°, 76.9°, and 77.3°, which were correlated with crystalline planes (012), (104), (110), (113), (024), (116), (211), (214), and (300), while the peaks at 2θ= 30.3°, 33.0°, 36.6°, 40.0°, 50.3°, 51.7°, 54.0°, 60.2°, 62.9°, 74.6°, and 78.5° corresponded to the tetragonal phase of zirconia. The monoclinic phase of zirconia was detected at 24.2°, 24.6°, 28.4°, 31.6°, 48.0°, 56.0°, 64.3°, 69.5°, and 75.3°. The appearance of comparatively large grains implied that the phase was most probably monoclinic, while the small inclusions were the tetragonal phase of zirconia. In addition, the tetragonal phase remained in the ceramic insert. It was possible to observe high-crystalline phases of Al$_2$O$_3$ and t-ZrO$_2$ with significantly sharp extended peaks. The finding suggested that using yttria as a stabilizing oxide caused phase stability in Al$_2$O$_3$-ZrO$_2$ ceramic. In this scenario, residual deformation within the ceramic due to the dilation effect may occur, resulting in significant influence due to strength fluctuations [22].

Grey relational analysis (GRA) methodology [39, 46]: in most machining operations, improving one output component by sacrificing the other is not attainable. Multi-objective optimization is extremely useful to draw critical decisions involving competing for output measured. A grey system represents the level of information that exists between the black (no information) state and the white (all information) state. The quality index grey relational grade (GRG) is used to characterize the correlation between the two states [43]. GRA approach reduces a multi-response problem into a single objective function (Fig. 4).

The machining parameters were optimized using grey relational analysis (GRA) and the analytic hierarchy process (AHP). The step-by-step procedure for GRA is described as follows: *Step 1* - data preprocessing: GRA begins by normalizing all of the responses and transforming them into a predetermined set of values between 0 and 1. The normalization of the output respondents is characterized by the specific objective [42]. This work aimed to minimize surface roughness (SR), tool flank wear (TFW), and tool wear loss (TWL) while maximizing the material removal rate (MRR). The goal of 'smaller-the-better' values for the surface roughness (SR), tool flank wear (TFW), and tool wear loss (TWL) while 'higher-the-better' values for material removal rate (MRR) were calculated using Eqs. A and B [39]:

$$Z_{ij} = \frac{\max(y_{ij}, i=1,2...n) - y_{ij}}{\max(y_{ij}, i=1,2...n) - \min(y_{ij}, i=1,2...n)} \quad \text{(A)}$$

$$Z_{ij} = \frac{y_{ij} - \max(y_{ij}, i=1,2...n)}{\max(y_{ij}, i=1,2...n) - \min(y_{ij}, i=1,2...n)} \quad \text{(B)}$$

where Z_{ij} is a normalized matrix, and y_{ij} is the experimental value. *Step 2* - grey relation coefficients (GRC) calculation: the preprocessed data based on the normalized sequences were then used to compute GRC using Eq. C [39]:

$$\gamma(Z_0, Z_{ij}) = \frac{\Delta\min + \xi\Delta\max}{\Delta_{oj}(k) + \xi\Delta\max} \quad \text{(C)}$$

where $\Delta\max$ and $\Delta\min$ are the highest and lowest value of the deviation sequence. The deviation sequence $\Delta_{oj}(k) = |[Z_0(k) - Z_{ij}(k)]|$. Here, $Z_0(k)$ represents the reference sequence and $Z_{ij}(k)$ represents the comparability sequence. The distinguishing coefficient (ξ) value can range from 0 to 1. In this investigation, it was chosen as 0.5. *Step 3* - grey relational grade (GRG) calculation: by assigning a weight value to each input parameter, GRG converts the multi-objective GRC to a single objective. The weighted GRG was calculated using Eq. D [39]:

$$GRG(Z_0, Z_{ij}) = \sum_{k=1}^{n} W_k \times \gamma(Z_0, Z_{ij}) \quad \text{(D)}$$

where $\sum_{k=1}^{n} W_k = 1$ is the weight of each parameter. The weight assignment to the input parameter was calculated by the analytical hierarchy process (AHP) [40] as follows: i) a pairwise comparison matrix A (m×m) was created as Eq. E [31]:

$$A_{m \times m} = \begin{bmatrix} 1 & A_{12} & A_{13} & ... & A_{ij} & ... & A_{1m} \\ A_{21} & 1 & A_{23} & ... & A_{2j} & ... & A_{2m} \\ A_{31} & A_{32} & 1 & ... & A_{3j} & ... & A_{3m} \\ ... & ... & ... & ... & ... & ... & ... \\ A_{i1} & A_{i2} & A_{i3} & ... & 1 & ... & A_{im} \\ ... & ... & ... & ... & ... & ... & ... \\ A_{m1} & A_{m2} & A_{m3} & ... & A_{mj} & ... & 1 \end{bmatrix} \quad \text{(E)}$$

where m denoted the number of performance measures taken into account. Each elemental relative score value of a matrix represents the relative importance rank of each character concerning the objective using the Saaty scale (Table VII) [40]. The values in the pairwise matrix were settled relevant to the adequacy of the objective, as shown in Table VIII. The values assigned to the row elements were compared to the values of the column elements in this case. An element value of 1 is given when the parameter is in relation to its own ($A_{ij}=1$ for i=j). A reciprocal element value is given when the parameter is relative to others ($A_{ij}=1/A_{ji}$). As a result, the matrix diagonal is assigned by a value of 1, the half matrix values are assigned by the relative importance of the individual qualities while the other half values are assigned based on the reciprocal of the consequent element. The comparison is done on a scale, highlighting how many times or how influential an output response is in comparison to other responses linked to the compared criteria or property. This study aimed to increase productivity and quality when turning Ti-6Al-4V. As

titanium alloys are considered hard-to-cut materials because of their low thermal conductivity, achieving close dimension tolerance with a good surface is critical. Thus, surface roughness is given the highest weight followed by material removal rate. For sustainability in machining and requirement of tool life, tool flank wear and tool wear loss were given equal weights. The pairwise comparison matrix established for the output responses is shown in Table VIII. ii) To compute the normalized weight (W_j) of the characteristics, the geometric mean (X_G) approach was used. The geometric mean and the normalized weight were determined from the pairwise matrix using Eqs. F and G [40]:

$$X_G = [\Pi_{j=1}^m a_{ij}]^{1/m} \tag{F}$$

$$W_j = \frac{X_{Gi}}{\Sigma_{i=1}^m X_{Gi}} \tag{G}$$

which calculated values are presented in Table IX. iii) Measuring consistency is critical because inconsistent factors do not result in excellent outcomes. The λ_{max} (maximum eigenvalue) was computed by summing relative values

column-wise, multiplying with the relevant normalized weights of the characteristics, and averaging the values. The consistency index (CI) for the pairwise matrix was calculated using Eq. H [40]:

$$CI = \frac{\lambda_{max} - n}{n-1} \tag{H}$$

where n is the number of parameters. The λ_{max} value calculated was 4.0733, with a consistency index (CI) of 0.0244. iv) The consistency ratio (CR) of the matrix was computed using Eq. I [40]:

$$CR = \frac{CI}{RI} \tag{I}$$

where the random index (RI) [40] for four parameters was chosen from Table X, which is 0.89 for n=4. As a result, the CR value for the current work was calculated as 0.0275. The value of CR determined from the pairwise matrix is used to determine the consistency of the assessment, and a value of 0.1 or less is generally deemed acceptable, reflecting a comprehensive examination of the present work. *Step 4 - calculation of grey relational grade (GRG):* using the AHP

Table VII - Saaty scale [31].

Rating scale	Definition	Explanation
1	Equal importance	Two activities contribute equally to the objective
3	Moderate importance	Experience and judgment slightly favor one activity over another
5	Strong importance	Experience and judgment strongly favor one activity over another
7	Very strong or demonstrated importance	An activity is favored very strongly over another; its dominance demonstrated in practice
9	Extreme importance	Evidence favoring one activity over another is of the highest possible order of affirmation
2, 4, 6, 8	Intermediate value	When compromise needed

Table VIII - The pairwise comparison matrix.

Response	Surface roughness (μm)	Tool flank wear (mm)	Material removal rate (mm^3/s)	Tool wear loss (g)
Surface roughness	1	7	5	7
Tool flank wear	1/7	1	1/3	1
Material removal rate	1/5	3	1	3
Tool wear loss	1/7	1	1/3	1

Table IX - Geometric mean and normalized weight of the output responses.

Response	Geometric mean (X_G)	Normalized weight (W_j)
Surface roughness	3.9563	0.6541
Tool flank wear	0.4671	0.0772
Material removal rate	1.1583	0.1915
Tool wear loss	0.4671	0.0772

Table X - Random index (RI) value based on the number of parameters.

n	1	2	3	4	5	6	7	8	9	10
RI	0	0	0.52	0.89	1.11	1.25	1.35	1.40	1.45	1.49

Table XI - Grey relation coefficient (GRC) and grey relational grade (GRG) calculated from the output responses.

Exp. No.	Cutting speed (rpm)	Feed rate (mm/rev.)	Depth of cut (mm)	GRC (SR)	GRC (TFW)	GRC (MRR)	GRC (TWL)	GRG
1	3500	0.05	0.1	0.3380	0.0772	0.0638	0.0772	0.5563
2	3500	0.10	0.2	0.3216	0.0615	0.0675	0.0521	0.5027
3	3500	0.15	0.3	0.2769	0.0531	0.0740	0.0402	0.4442
4	3500	0.20	0.4	0.2545	0.0436	0.0849	0.0368	0.4198
5	3500	0.25	0.5	0.2180	0.0382	0.1044	0.0368	0.3974
6	3625	0.05	0.4	0.4306	0.0351	0.0686	0.0393	0.5735
7	3625	0.10	0.5	0.3401	0.0325	0.0810	0.0299	0.4835
8	3625	0.15	0.1	0.4336	0.0488	0.0668	0.0611	0.6103
9	3625	0.20	0.2	0.3815	0.0429	0.0762	0.0528	0.5535
10	3625	0.25	0.3	0.3290	0.0377	0.0967	0.0472	0.5105
11	3750	0.05	0.2	0.4964	0.0390	0.0659	0.0411	0.6425
12	3750	0.10	0.3	0.4012	0.0341	0.0748	0.0340	0.5441
13	3750	0.15	0.4	0.3679	0.0310	0.0945	0.0315	0.5249
14	3750	0.20	0.5	0.3295	0.0298	0.1475	0.0285	0.5353
15	3750	0.25	0.1	0.4311	0.0423	0.0719	0.0553	0.6006
16	3875	0.05	0.5	0.4979	0.0265	0.0742	0.0267	0.6252
17	3875	0.10	0.1	0.5371	0.0370	0.0667	0.0506	0.6913
18	3875	0.15	0.2	0.4841	0.0339	0.0772	0.0380	0.6331
19	3875	0.20	0.3	0.4140	0.0305	0.1024	0.0330	0.5799
20	3875	0.25	0.4	0.3651	0.0276	0.1915	0.0287	0.6128
21	4000	0.05	0.3	0.6541	0.0292	0.0702	0.0330	0.7865
22	4000	0.10	0.4	0.5630	0.0266	0.0903	0.0276	0.7074
23	4000	0.15	0.5	0.4876	0.0257	0.1536	0.0257	0.6927
24	4000	0.20	0.1	0.6414	0.0355	0.0736	0.0459	0.7964
25	4000	0.25	0.2	0.5519	0.0314	0.1027	0.0397	0.7258

SR: surface roughness; TFW: tool flank wear; MRR: material removal rate; TWL: tool wear loss.

normalized weights (Table IX) and GRC value of each output response, GRG was calculated by employing Eq. J [39]; the GRG calculated using these weights of each experimental trial is displayed in Table XI.

$$GRG = \frac{0.6541.GRC(SR)+0.0772.GRC(TFW)+}{0.1915.GRC(MRR)+0.0772.GRC(TWL)} \quad (J)$$

RESULTS AND DISCUSSION

The results of the output factors (SR, TFW, MRR, and TWL) were evaluated to access how cutting parameters (v, f, and d) affected these responses. The main effects of each machining parameter are shown in Fig. 5. Fig. 5a indicates that with the

rise of both the feed rate and depth of cut, there was a rise in the value of surface roughness. Pervaiz et al. [17] stated that such a statistical trend was observed, which was attributed to the fact that just a little amount of material was plowed at a shallow depth of cut with low feed rates. At low feed rates, the uncut chip thickness was low, and this standard can reduce plunging and be labeled as having a favorable low value of surface roughness [19]. On contrary, increasing the feed rate caused an increase in the plunging effect, which was integrated with a poor surface quality finish. The value of cutting speed increase was more promising for improving surface roughness. The mean effect plot in Fig. 5b reveals a steeper inclination curve for cutting speed and depth of cut, indicating that increasing these parameters led

to increased tool flank wear. With an increase in depth of cut due to the thermal effect, there is an increase in cutting temperature and thermal stress, increasing flank wear [18]. As shown in the mean effect plot in Fig. 5c, increasing the feed rate and depth of cut increased the material removal rate. When turning at high cutting speeds and high depth of cut as shown in the mean effect plot of Fig. 5d, the gradual tool wear, strain hardening effect generated by high plastic deformation while turning operation, and material adherence at the tool-workpiece interface all result in high tool wear loss. From Fig. 5, the nearly identical steep hill curve pattern for the depth of cut for all four output measures (SR, TFW, MRR, and TWL) indicated that the output value increased as the depth of cut increased. The SR, TFW, and MRR

increased, and TWL decreased with an increase in feed rate. However, an increase in cutting speed decreased the SR and MRR and increased the TFW and TWL.

Table XII shows the best and worst output responses for all experiment trials. Different parameter settings in the turning process are required to attain excellent output responses. The desired output value for SR, TFW, and TWL should attain the minimum value whereas, for MRR, it is the maximum. As these parameter settings differ in producing the optimal responses, a robust multi-objective optimization is required for decision-making in machining operations. The grey relational grade (GRG) was used to evaluate the multi-response quality characteristics, and a higher GRG value
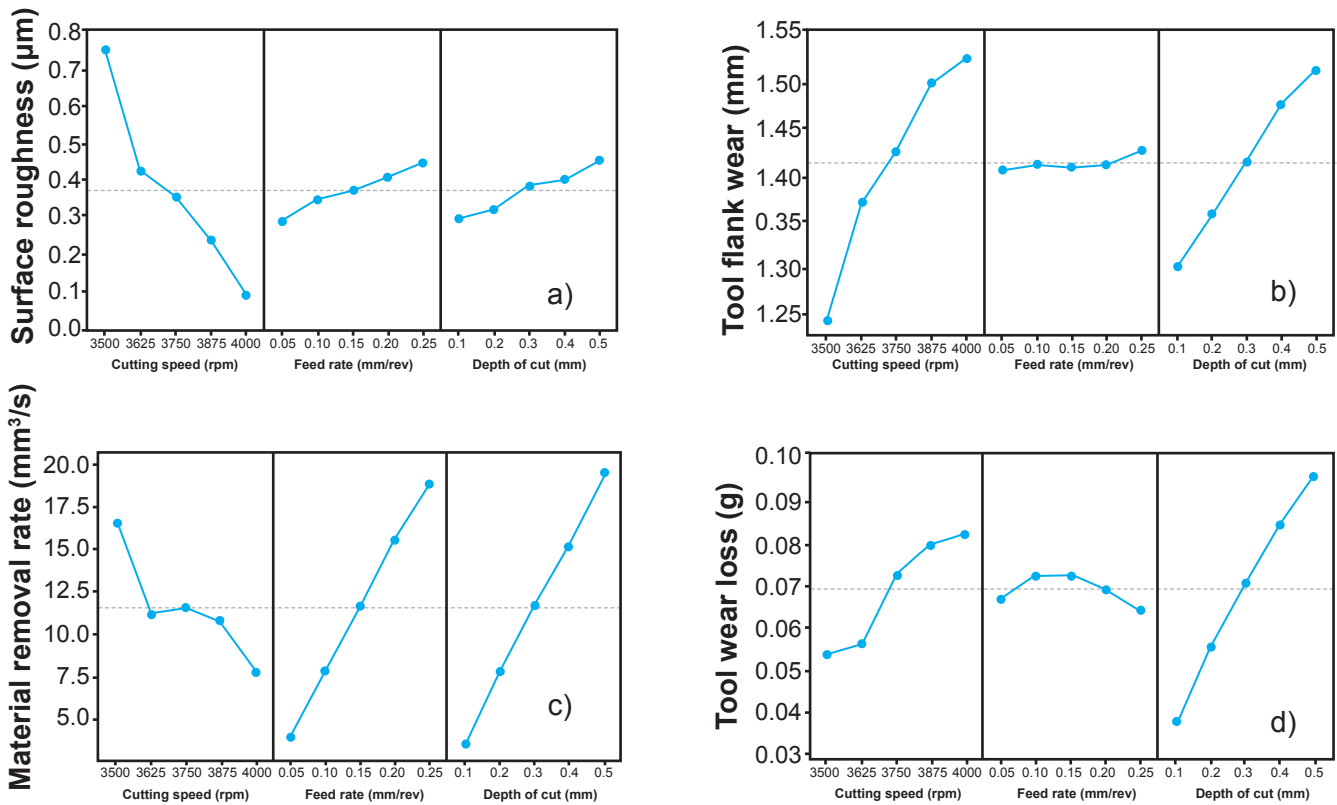

Figure 5: Main effects plot (data means) for: a) surface roughness (SR); b) tool flank wear (TFW); c) material removal rate (MRR); and d) tool wear loss (TWL).

Table XII - The best and worst output responses for all experiment trials.

Response	Output		Cutting speed, v (rpm)	Feed rate, f (mm/rev.)	Depth of cut, d (mm)
Surface roughness	Best	0.285	4000	0.05	0.3
	Worst	0.959	3500	0.25	0.5
Tool flank wear	Best	1.118	3500	0.05	0.1
	Worst	1.619	4000	0.15	0.5
Material removal rate	Best	29.333	3875	0.25	0.4
	Worst	0.836	3500	0.05	0.1
Tool wear loss	Best	0.021	3500	0.05	0.1
	Worst	0.112	40000	0.15	0.5

was preferred regardless of the type of quality feature. GRG provides a single measure for multiple quality parameters, having higher GRG values yielding higher output features [41]. The highest value of GRG was measured for the 24th trial, implying that the optimal process parameters are near the operating state for that experiment run.

Regression model for GRG function [34]: a quadratic second-order polynomial model of response surface methodology (RSM) was created for a multi-objective GRG function, which accurately describes the GRG computed from the experiment results. The concise mathematical model is shown in Eq. K, including all the insignificant terms. The proposed model is only applicable to turning Ti-6Al-4V using alumina-zirconia (Al_2O_3-ZrO_2) ceramic insert with the given machine tool, and the dry machining condition under the conditions used ($3000 \leq$ v ≤ 4000 rpm, $0.05 \leq$ f ≤ 0.25 mm/rev., $0.1 \leq$ d ≤ 0.5 mm).

$$GRG = \begin{matrix} 0.5342+0.09943.v-0.03722.f-0.06053d+ \\ 0.0419.v.v+0.0295.f.f+0.0275 .d.d- \\ 0.0289.v.f-0.0238.v.d-0.0124.f.d \end{matrix} \quad (K)$$

Model validity and fitness test [42]: the validity of the created mathematical model was estimated by the use of the percentage variation (θ_i) and average percentage variation ($\overline{\theta_i}$) expressed as [42]:

$$\theta_i = \left(\frac{GRG_P - GRG_E}{GRG_E} \right).100 \quad (L)$$

$$\overline{\theta_i} = \left[100 - \frac{\sum_{i=1}^{N} \theta_i}{N} \right] \quad (M)$$

where GRG_P is the predicted outcome obtained by the mathematical model, GRG_E is the actual outcome measured by experimental data, and N is the size of the experimental data. Eqs. L and M were used to test the accuracy of the developed mathematical model. In this study, for $\Sigma\theta_i$=3.479 and N=25, the average percentage variation (Eq. M) revealed that the developed mathematical model could accurately estimate the GRG value with 99.86% accuracy.

The significance of the process parameters and the fitness of the model in developing a statistical relationship between the outcomes and the machining parameters were established using analysis of variance (ANOVA) [38]. As presented in Table XIII, ANOVA was explored at the confidence level of 95% to analyze the influence of the machining parameters. The R^2 value indicated that the model accurately explained 97.49% of the total variations. From the ANOVA table it was identified that all linear (v, f, d) parameters were significant while quadratic (v.v, f.f, d.d) and interaction (v.f, v.d, f.d) parameters were non-significant. The cutting speed was the highest significant parameter affecting GRG among the turning experiment settings with 79.35% followed by the depth of cut (12.92%) and feed rate (3.76%). The quadratic factors had a total of 3.80% contribution while interaction parameters had a 0.18% contribution.

Figs. 6a to 6c present contour and surface graphs of GRG for the turning operation. These curves illustrate the correlation of the machining parameters to the calculated GRG value. The highest value of the GRG was retrieved at maximum cutting speed with minimum feed rate and a minimum depth of cut. Fig. 6d compares the GRG experimental collected from the experiments and GRG predicted values calculated from the developed regression

Table XIII - ANOVA for response surface model.

| Source	DF	Adj SS	Adj MS	F-value	p-value	% contribution	
Regression	9	0.2536	0.0282	34.4	0.000	95.38	
Linear	3	0.2084	0.2084	254.4	0.007	96.02	
v	1	0.1722	0.1722	210.2	0.000	79.35	Significant
f	1	0.0082	0.0082	10.0	0.007	3.76	Significant
d	1	0.0280	0.0280	34.2	0.000	12.92	Significant
Quadratic	3	0.0082	0.0082	10.1	0.298	3.80	
v.v	1	0.0036	0.0036	4.5	0.052	1.68	
f.f	1	0.0028	0.0028	3.4	0.084	1.30	
d.d	1	0.0018	0.0018	2.2	0.162	0.82	
Interaction	3	0.0004	0.0004	0.5	2.196	0.18	
v.f	1	0.0000	0.0000	0.0	0.920	0.00	
v.d	1	0.0002	0.0002	0.2	0.675	0.07	
f.d	1	0.0002	0.0002	0.3	0.601	0.11	
Error	15	0.0123	0.0008			4.62	
S: 0.0358		R^2: 97.49%				R^2(adj.): 95.78%	
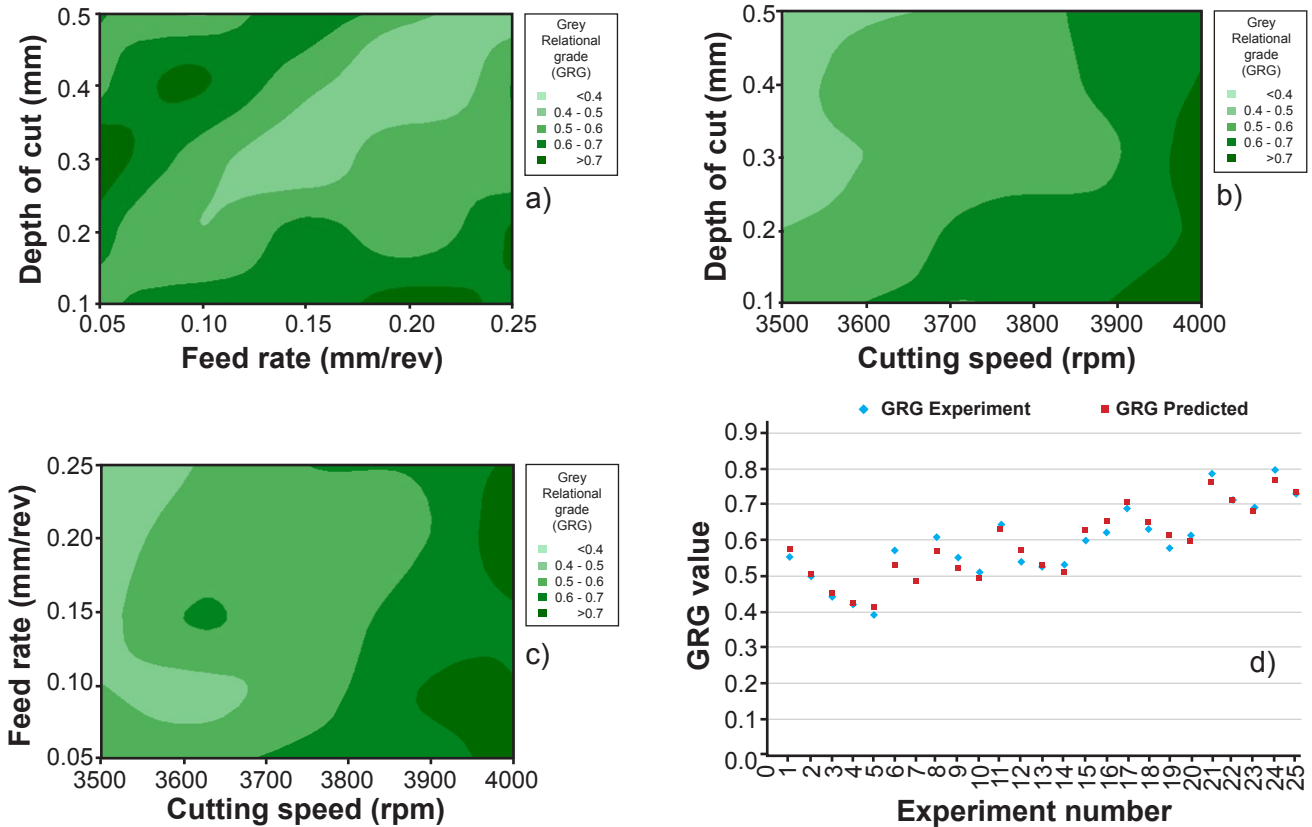
Figure 6: Contour and surface graphs of GRG for the turning operation (a-c) and comparison of GRG experiment and GRG predicted values (d).

model having a maximum mean error of 3.47%. At the highest value of GRG, the shear force with the shear plane diminished at higher levels of feed rate, depth of cut, and lower cutting speed, resulting in an enhanced MRR but diminished SR, TFW, and TWL. The chip friction increases at a high feed rate and high depth of cut, resulting in an increased temperature and thermal stresses at the tool-chip interface, resulting in a rough surface [41]. The adverse impact of high feed rate and high depth of cut is conserved by high cutting speed [17]; as a result, the highest value of GRG was attained by experiment number 24 (input factors cutting speed, feed rate, and depth of cut set at 4000 rpm, 0.2 mm/rev. and 0.1 mm, respectively).
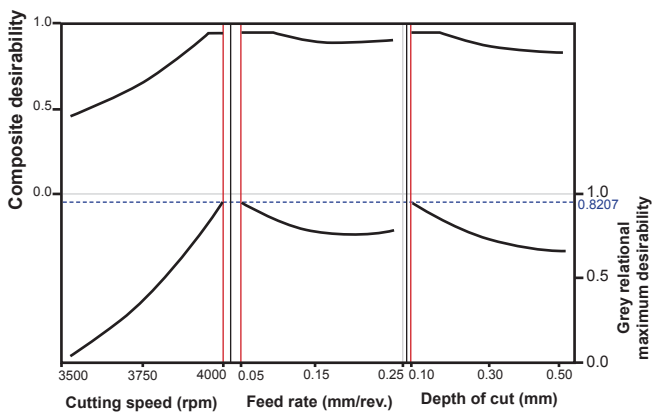

Figure 7: Graphs of optimized results for maximum GRG value

Optimization of the GRG response surface model: the developed RSM mathematical model for GRG was employed to predict the optimal machining parameters when the grey relation grade was set for maximum value. Fig. 7 displays the composite desirability as 0.8207, very close to 1.0, which indicated optimized machining settings for grey relational maximum value attained when cutting speed, feed rate, and depth of cut were set as 4000 rpm, 0.05 mm/rev., and 0.1 mm, respectively.

Confirmation experiment: the comparison of the optimum turning process parameters from the GRG RSM model and the best experimental trial of the L_{25} orthogonal array is given in Table XIV. The results showed a 10.31% decrease in surface roughness, 6.51% decrease in tool flank wear, 2.21% rise in MRR and a 7.69% increase in tool wear loss. The only parameter difference between the best experimental trial and the optimum trial was the feed rate, while the cutting speed and depth of cut were the same in both trials. To address multi-objective problems, it is critical to assess machining parameters during the machining process. As presented in Table XIV, when comparing the output results of surface roughness for both the trial runs, the surface quality improved with higher cutting speeds because there were fewer chances of built-up edge creation. On the other hand, an increase in the depth of cut and feed rate deteriorated the surface quality. When all of the input parameters (cutting speed, feed rate, and depth of cut) were set to their maximum level, the MRR increased. In

Table XIV - Comparison of experimental best trial and optimum trial.

	Machining setting			Output response			
	Cutting speed (rpm)	Feed rate (mm/rev.)	Depth of cut (mm)	Surface roughness (µm)	Tool flank wear (mm)	Material removal rate (mm³/s)	Tool wear loss (g)
Best trial	4000	0.20	0.1	0.291	1.412	3.671	0.052
Optimum trial	4000	0.05	0.1	0.261	1.320	3.590	0.048
Change				10.31% decrease	6.51% decrease	2.21% decrease	7.69% decrease

comparison to the best trial, MRR for the optimized trial indicated a 2.21% reduction in material removal rate. The only variance between the two best and optimum trials (Table XIV) was that the feed rate was reduced, resulting in a lower MRR value. This is because, at lower feed rates, the turning mechanics do not shift from rubbing action to shearing action. In comparison to the best trial, tool flank wear and tool wear loss for the optimal trial decreased by 6.51% and 7.69%, respectively. Increasing the feed rate and depth of cut result in more friction, which raises the cutting temperature and triggers the flank wear and tool wear. In the machining process, proper integration of machining parameters can lead to the optimum multi-response output.

CONCLUSIONS

In this study, Ti-6Al-4V alloy was turned on a CNC machine using an alumina-zirconia (Al$_2$O$_3$-ZrO$_2$) ceramic insert. Cutting speed (v), feed rate (f), and depth of cut (d) each at five different levels were selected as the input machining factors. Surface roughness (SR), tool flank wear (TFW), material removal rate (MRR), and tool wear loss (TWL) were examined as quality attributes. The experiments were carried out using Taguchi's L$_{25}$ design. To achieve a sustainable machining process, optimal parameters were obtained using multi-objective optimization. Based on grey Taguchi-based response surface methodology (GT-RSM), the following can be concluded. i) Grey relation analysis (GRA) is a structured optimization methodology that is effectively employed for multi-objective optimization of machining parameters. This technique is easy to perform because it does not involve a large amount of computation theory and calculations. The GT-RSM method was successfully used in combination with the analytical hierarchy process (AHP) weight approach for multi-objective analysis using grey relational grade (GRG) to determine the optimal interpretation of machining parameters for the Ti-6Al-4V alloy. The optimum condition for the highest GRG value was attained when cutting speed, feed rate, and depth of cut were 4000 rpm, 0.2 mm/rev., and 0.1 mm, respectively. ii) According to the ANOVA results, cutting speed with a contribution of 79.35% had the highest influence on the machining responses (SR, TFW, MRR, and TWL) of all the input process parameters studied, followed by the depth of cut and feed rate with 12.92% and 3.76% contributions,

respectively. iii) A quadratic mathematical model was formulated through response surface methodology (RSM). The R^2 value of 97.49% and the average variation of 99.86% for the developed mathematical model were used to assess the models' accuracy. GRG experimental values and GRG predicted values calculated from the developed regression model had a mean error of 3.47%. All of this validated that the proposed method had an excellent fit and can estimate multi-objective values that are rationally close to the experimental values. iv) The optimum trial revealed an enhancement of 10.31% in surface roughness, 6.51% in tool flank wear, and 7.69% in tool wear loss with a reduction of 2.21% in material removal rate. Dry machining can promote sustainable green manufacturing by selecting the correct level of cutting speed, feed rate, and depth of cut to improve product quality, tool life, manufacturing lead time, energy, and cost. Future studies can integrate the impact of chip morphology, tool chattering, fatigue behavior, and specific cutting energy to determine the correct combination of the machining parameters. Cutting forces and morphological changes can also be studied concerning the type of cutting tool, its material, and its geometry. The proposed multi-objective optimization methodology can be employed to enhance the sustainability of other machining and manufacturing techniques.

REFERENCES

[1] K. Weinert, I. Inasaki, J.W. Sutherland, T. Wakabayashi, CIRP Ann. Manuf. Technol. **53** (2004) 511.

[2] G. Byrne, E. Scholta, CIRP Ann. Manuf. Technol. **42** (1993) 471.

[3] T. Ueda, A. Hosokawa, K. Yamada, J. Manuf. Sci. Eng. Trans. ASME **128** (2006) 130.

[4] Z. Chen, K. Wong, W. Li, S.Y. Liang, D.A. Stephenson, J. Manuf. Sci. Eng. Trans. ASME **123** (2001) 506.

[5] A. Devillez, G. Le Coz, S. Dominiak, D. Dudzinski, J. Mater. Process. Technol. **211** (2011) 1590.

[6] J.A. Ghani, M. Rizal, C.H. Che Haron, J. Clean. Prod. **85** (2014) 289.

[7] X. Ji, B. Li, X. Zhang, S.Y. Liang, Int. J. Precis. Eng. Manuf. **15** (2014) 2443.

[8] S. Sivarajan, R. Padmanabhan, Procedia Eng. **97** (2014) 15.

[9] B. Wang, Z. Liu, Int. J. Adv. Manuf. Technol. **98** (2018)

1925.

[10] C. Camposeco-Negrete, J. Clean. Prod. **91** (2015) 109.

[11] N. Narutaki, Y. Yamane, S. Tashima, H. Kuroki, CIRP Ann. Manuf. Technol. **46** (1997) 43.

[12] R. Suresh, S. Basavarajappa, V.N. Gaitonde, G.L. Samuel, Int. J. Refract. Met. Hard Mater. **33** (2012) 75.

[13] V. Chavan, S. Kadam, M. Sadaiah, Mater. Manuf. Process. **34** (2019) 8.

[14] T.F. Ariff, F.F. Zolkapli, F.A. Sapuan, A.Z.A. Azhar, Rubina Bahar, A.N. Mustafizul Karim, A.K.M. Nurul Amin, J. Eng. Res. Appl. **8** (2018) 51.

[15] J. Liu, X. Ji, Z. Guo, C. Qin, Y. Xiao, Q. You, J. Mater. Res. Technol. **9** (2020) 1389.

[16] Ş. Şirin, M. Sarikaya, Ç.V. Yildirim, T. Kivak, Tribol. Int. **153** (2020) 2021.

[17] S. Pervaiz, A. Rashid, I. Deiab, M. Nicolescu, Mater. Manuf. Process. **29** (2014) 219.

[18] D. Yang, Z. Liu, Materials **9** (2016) 1.

[19] A.T. Abbas, N. Sharma, S. Anwar, M. Luqman, I. Tomaz, H. Hegab, Materials **13** (2020) 1.

[20] M.M. Basha, S.M. Basha, B.K. Singh, N. Mandal, M.R. Sankar, Mater. Today Proc. **26** (2019) 534.

[21] B. Basu, Int. Mater. Rev. **50** (2005) 239.

[22] M. Arin, G. Goller, J. Vleugels, K. Vanmeensel, J. Mater. Sci. **43** (2008) 1599.

[23] Y. Dyatlova, S.S. Ordanyan, A. Osmakov, V. Pesin, V. Rumyantsev, Adv. Sci. Technol. **65** (2010) 11.

[24] F. Qunbo, W. Fuchi, Z. Huiling, Z. Feng, Mol. Simul. **34** (2008) 1099.

[25] A. Kuwabara, T. Tohei, T. Yamamoto, I. Tanaka, Phys. Rev. B Condens. Matter **71** (2005) 1.

[26] J. Chevalier, L. Gremillard, A.V. Virkar, D.R. Clarke, J. Am. Ceram. Soc. **92** (2009) 1901.

[27] D. Gutknecht, J. Chevalier, V. Garnier, G. Fantozzi, J. Eur. Ceram. Soc. **27** (2007) 1547.

[28] J. Chevalier, J.M. Drouin, B. Cales, J. Am. Ceram. Soc. **82** (1999) 2150.

[29] Y. Shin, Y. Rhee, S. Kang, J. Am. Ceram. Soc. **82** (1999) 1229.

[30] M. Szutkowska, J. Mater. Process. Technol. **153** (2004) 868.

[31] B. Zhao, H. Liu, C. Huang, J. Wang, B. Wang, Y. Hou, Int. J. Adv. Manuf. Technol. **102** (2019) 3431.

[32] F.P. Damir Grguraš, M. Kern, Procedia CIRP **77** (2018) 630.

[33] Z.W. Chen, D.W. Tan, W.M. Guo, H.T. Lin, J. Synth. Cryst. **47** (2018) 12.

[34] X. Tian, J. Zhao, H. Yang, Z. Wang, H. Liu, Int. J. Adv. Manuf. Technol. **100** (2019) 401.

[35] A. Altin, M. Nalbant, A. Taskesen, Mater. Des. **28** (2007) 2518.

[36] R.P. Zeilmann, F. Fontanive, R.M. Soares, Int. J. Adv. Manuf. Technol. **92** (2017) 2705.

[37] T. Roy, R.K. Dutta, Soft Comput. **23** (2019) 5053.

[38] S. Kumar, R.N. Yadav, R. Kumar, Int. J. Precis. Technol. **9** (2020) 71.

[39] H. Patel, J. Patel, B. Gajera, H. Rana, Reliab. Theory Appl. **16** (2021) 276.

[40] J.D. Patel, K.D. Maniya, Mater. Today Proc. **2** (2015) 2496.

[41] C.J. Tzeng, Y.H. Lin, Y.K. Yang, M.C. Jeng, J. Mater. Process. Technol. **209** (2009) 2753.

[42] S. Singh, I. Singh, A. Dvivedi, Proc. Inst. Mech. Eng. B J. Eng. Manuf. **227** (2013) 1767.

[43] A.N. Haq, P. Marimuthu, R. Jeyapaul, Int. J. Adv. Manuf. Technol. **37** (2008) 250.

[44] T. Rajmohan, K. Palanikumar, J. Compos. Mater. **46** (2012) 869.

[45] V.N. Gaitonde, S.R. Karnik, J.C.C. Rubio, W.O. Leite, J.P. Davim, J. Compos. Mater. **48** (2014) 21.

[46] R. Adalarasan, M. Santhanakumar, M. Rajmohan, Int. J. Adv. Manuf. Technol. **78** (2015) 1161.